Global Health Care
WISDOM ACADEMIC https://doi.org/10.63808/ghc.v2i1.535 Volume 2 , Issue 1

Research Article

Lactate Metabolic Reprogramming Reverses CD8+ T Cell Exhaustion: A New Target for Cancer Immunotherapy

Gang Liu[1,*], Jia Wang[2], Alena Mikalaeuna Vasiukevich[1], Biao Feng[3], Liqiang An[4]
[1]International Sakharov Environmental Institute, Belarusian State University, Minsk 220114, Belarus
[2]Taishan Polytechnic, Tai'an 271000, China
[3]Belarusian State University, Minsk 220114, Belarus
[4]Volgograd State Pedagogical University, Volgograd 400005, Russia
[*]**Correspondence:** Gang Liu, lg6666699@163.com

© The Author(s) 2026.
This article is published by Wisdom Academic Press Ltd. under a Creative Commons Attribution 4.0 International License. The license permits use, sharing, adaptation, distribution, and reproduction in any medium or format, provided that appropriate credit is given to the original author(s) and the source, a link to the license is supplied, and any modifications are indicated. Unless otherwise stated, all images and third-party materials included in this article are also covered by the same license. For any material not covered by this license, if the intended use is neither permitted by applicable law nor allowed under the license terms, direct permission must be obtained from the copyright holder. To view a copy of this license, please visit http://creativecommons.org/licenses/by/4.0/.

Abstract

Lactate accumulation in the tumor microenvironment is an important factor inducing CD8+ T cell exhaustion and immunotherapy resistance, but whether reprogramming lactate metabolism can reverse CD8+ T cell exhaustion remains unclear. This study aims to explore the effects of targeted lactate metabolism on CD8+ T cell function and anti-tumor immunotherapy. Single-cell RNA sequencing, metabolomics, flow cytometry, and immunohistochemistry were used to analyze the lactate metabolism characteristics and exhaustion phenotypes of tumor-infiltrated CD8+ T cells; Genetics or pharmacological methods were used to regulate lactate dehydrogenase A (LDHA) and the lactate transporter MCT1/4, and to evaluate anti-tumor effects and synergistic effects with anti-PD-1 therapy in tumor-bearing mouse models of B16-OVA and MC38. Lactate uptake in tumor-infiltrating CD8+ T cells increases, with significant upregulation of MCT1/4 and LDHA, accompanied by decreased mitochondrial membrane potential, impaired oxidative phosphorylation, and increased expression of depletion markers such as PD-1, TIM-3, LAG-3, and TOX/NR4A. Inhibiting LDHA or blocking MCT1/4 lowers intracellular lactate levels, restores mitochondrial function and oxidative phosphorylation, enhances secretion of IFN-γ, TNF-α, and granzyme B, and downregulates depletion-related transcriptional programs. In tumor-bearing mice, reprogramming of lactate metabolism significantly inhibits tumor growth, increases the proportion of tumor-infiltrating CD8+ T cells and effector memory phenotypes, and produces synergistic effects with anti-PD-1 therapy. Mechanistically, lactate regulates the expression of exhaustion-related genes through histone lactation modification, while metabolic intervention can reverse this epigenetic program. Targeted lactate

metabolism reprogramming can effectively reverse $CD8^+$ T cell exhaustion, enhance the efficacy of tumor immunotherapy, and provide new potential targets for solid tumor immunotherapy.

Keywords

Lactate metabolism, $CD8^+$ T cell depletion, Tumor microenvironment, Immunotherapy, Metabolic reprogramming, MCT1/4, Histone lactation, Anti-PD-1

1. Introduction

Tumor immunotherapy, especially the use of immune checkpoint inhibitors (ICIs), has significantly changed the treatment landscape for various cancers. However, primary or acquired resistance to ICIs in most solid tumor patients remains a major challenge in the clinic. $CD8^+$ T cells are the main effector cells that drive anti-tumor immunity, and their infiltration, functionality, and persistence directly determine how effective immunotherapy will be. But in the tumor microenvironment (TME), $CD8^+$ T cells often gradually lose their ability to proliferate and function, showing sustained high levels of inhibitory receptors like PD-1, TIM-3, and LAG-3, along with upregulation of exhaustion-associated transcription programs like TOX and NR4A, eventually reaching an 'exhausted' state. So, figuring out what drives $CD8^+$ T cell exhaustion and finding ways to reverse it is key to improving responses to cancer immunotherapy.

In recent years, research on immunometabolism has shown that metabolic competition and accumulation of metabolic products in the tumor microenvironment (TME) are key factors leading to T cell dysfunction. Tumor cells tend to ramp up glycolysis even under high oxygen conditions-a phenomenon known as the 'Warburg effect'-resulting in a large amount of lactate production that is expelled outside the cell through monocarboxylate transporters (MCTs). This lactate-rich environment not only promotes tumor growth, angiogenesis, and the recruitment of immunosuppressive cells, but also directly affects $CD8^+$ T cells. Previous studies often treated lactate as just a metabolic waste, but new evidence shows that lactate can act as an important signaling molecule and metabolic substrate, helping to regulate immune cell fate and function. In tumor-infiltrating $CD8^+$ T cells, lactate dehydrogenase A (LDHA) and lactate transporters MCT1/4 are upregulated, suggesting active lactate metabolic reprogramming. However, it's still unclear whether this reprogramming actually enhances or suppresses the antitumor function of $CD8^+$ T cells and whether targeting lactate metabolism can reverse T cell exhaustion.

On a mechanistic level, lactate not only affects intracellular pH, redox balance, and mitochondrial function, but can also link metabolic states to gene expression through epigenetic modifications like histone lactylation. Histone lactylation has been shown to be involved in macrophage polarization, tumor progression, and immune regulation, but whether it plays a role in establishing and maintaining

the transcriptional programs associated with $CD8^+$ T cell exhaustion still lacks systematic study. At the same time, inhibiting LDHA or blocking MCT1/4 has shown antitumor potential in some tumor models, but how much these effects rely on intrinsic lactate metabolism remodeling in $CD8^+$ T cells, and whether they can synergize with anti-PD-1 therapy, still needs more in-depth verification. Most current studies focus on tumor cells or immunosuppressive myeloid cells, with relatively limited attention to lactate metabolism reprogramming in $CD8^+$ T cells themselves, and there is a lack of systematic evidence combining single-cell analysis, metabolomics, and functional validation.

Based on the background above, this study proposes a core hypothesis: lactate from the TME drives metabolic reprogramming and histone lactylation in $CD8^+$ T cells, which in turn promotes the exhaustion program; targeting LDHA/MCT1/4 to inhibit lactate production or uptake could restore mitochondrial function and oxidative phosphorylation in $CD8^+$ T cells, reverse the exhausted phenotype, and enhance the effectiveness of anti-tumor immunotherapy. To test this hypothesis, we plan to integrate single-cell RNA sequencing, metabolomics, flow cytometry, epigenetic analysis, and tumor-bearing mouse models to systematically analyze lactate metabolism patterns in tumor-infiltrating $CD8^+$ T cells, evaluate the effects of genetic or pharmacological intervention of LDHA/MCT1/4 on T cell exhaustion and anti-tumor immunity, and further explore their synergy with anti-PD-1 therapy and the mechanisms of histone lactylation.

So, this study aims to answer the following scientific questions: What kind of lactate metabolism reprogramming happens in tumor-infiltrating $CD8^+$ T cells? Can targeting lactate metabolism reverse $CD8^+$ T cell exhaustion and boost anti-tumor immunity? Does histone lactylation mediate the regulation of exhaustion-related gene expression by lactate? Can interventions in lactate metabolism sensitize anti-PD-1 therapy? The results of this study will reveal the key role of lactate metabolism reprogramming in $CD8^+$ T cell exhaustion and provide new metabolism-epigenetic intervention targets for solid tumor immunotherapy.

2. Literature Review

2.1. Tumor immunotherapy and $CD8^+$ T cell exhaustion

$CD8^+$ T cells are key effector cells in anti-tumor immunity, and their functional state directly affects the clinical effectiveness of immune checkpoint inhibitors (ICIs). However, under chronic antigen stimulation and in the immunosuppressive tumor microenvironment (TME), $CD8^+$ T cells gradually become exhausted, showing reduced proliferation, decreased secretion of effector cytokines, weakened cytotoxicity, and sustained high expression of inhibitory receptors like PD-1, TIM-3, and LAG-3 (Wherry, 2011). Metabolic remodeling of the tumor microenvironment, infiltration of immunosuppressive cells, and activation of inhibitory signaling pathways jointly promote this process (Hanahan & Weinberg, 2011). In recent years, the transcription factor TOX has been confirmed as a

key molecule driving the exhaustion of $CD8^+$ T cells, as it establishes and maintains the expression of exhaustion-related genes through epigenetic programs (Khan et al., 2019). Additionally, NR4A family transcription factors have been found to limit CAR-T cell function in solid tumors, suggesting that depletion programs have a multi-level transcriptional regulatory network (Chen et al., 2019). So, figuring out what drives $CD8^+$ T cell exhaustion and finding effective ways to reverse it is key to boosting the response rate to immunotherapy in solid tumors.

2.2. Lactate metabolism and immune suppression in the tumor microenvironment

Tumor cells prefer glycolysis even when there's plenty of oxygen, known as the Warburg effect, which leads to the production of a lot of lactic acid that gets released into the tumor microenvironment (TME) (Warburg, 1956). Lactic acid from tumors isn't just a metabolic waste; it can also act as a signaling molecule to reshape immune cell functions. For example, tumor-derived lactic acid can push tumor-associated macrophages to polarize toward an M2-like immunosuppressive phenotype (Colegio et al., 2014). Earlier studies have found that lactate from tumor cells can significantly suppress human T cell proliferation and cytokine secretion (Fischer et al., 2007). Further research showed that lactate dehydrogenase A (LDHA)-mediated lactate production can weaken the tumor immune surveillance functions of T cells and NK cells, while inhibiting LDHA can partially restore anti-tumor immunity (Brand et al., 2016). These findings indicate that the lactate-enriching microenvironment is a key metabolic factor leading to $CD8^+$ T cell dysfunction.

2.3. Lactate transport and T cell metabolic reprogramming

Lactic acid distribution inside and outside cells is regulated by the monocarboxylate transporter (MCT) family, with MCT1 and MCT4 playing key roles in tumor and immune cell metabolism (Halestrap, 2012). TCell activation, differentiation, and effector functions heavily rely on metabolic reprogramming, and the balance between glycolysis, oxidative phosphorylation, and fatty acid oxidation determines T cell fate (Buck et al., 2015). In exhausted $CD8^+$ T cells, PD-1 signaling can suppress glycolysis and promote fatty acid oxidation, leading to energy shortage (Bengsch et al., 2016). Patsoukis et al. (2015) further found that PD-1 alters T cell metabolic processes by inhibiting glycolysis and promoting lipolysis and fatty acid oxidation. Additionally, continuous antigen stimulation impairs mitochondrial oxidative phosphorylation, limiting T cell self-renewal and promoting exhaustion (Vardhana et al., 2020). However, systematic studies remain on how tumor-infiltrating $CD8^+$ T cells uptake and utilize lactic acid, and whether targeting MCT1/4 or LDHA can reverse depletion.

2.4. Histone lactation: A bridge between metabolism and epigenetics

In 2019, Zhang and others (2019) first reported that histone lactylation is a new type of epigenetic

modification that links metabolic states to gene expression. Lactate can drive histone lysine lactylation and regulate gene transcription. Subsequently, Xiong et al. (2022) found that lactation-driven METTL3-mediated RNA m6A modification can promote the immunosuppressive function of tumor-infiltrating myeloid cells. These studies suggest that lactate not only affects T cell function through metabolic pathways, but might also shape the exhaustion program of $CD8^+$ T cells through epigenetic mechanisms like histone lactylation. However, it's still unclear whether histone lactylation is involved in the sustained expression of genes related to $CD8^+$ T cell exhaustion, and whether metabolic interventions can reverse this epigenetic program.

2.5. Limitations of existing research and the contribution of this study

In summary, existing research has revealed the important role of lactate in tumor immunosuppression and preliminarily established a link between lactate metabolism and T cell dysfunction. However, the following shortcomings remain: most studies focus on tumor cells or myeloid cells, with insufficient attention to reprogramming of autolactate metabolism in CD8-T cells; The causal mechanisms between lactate uptake, intracellular metabolism, and transcriptional depletion remain unclear; There is a lack of direct evidence whether histone lactation mediates the expression of genes related to $CD8^+$ T cell exhaustion; Whether targeting LDHA/MCT1/4 can synergistically enhance anti-PD-1 therapy remains to be verified.

In addition, in recent years, there have been several new developments in the field of tumor immunology that haven't yet been effectively integrated with the reprogramming of $CD8^+$ T cell lactate metabolism and histone lactylation mechanisms. For example, CRISPR screening and single-cell multi-omics have identified new immune checkpoints on tumor-infiltrating regulatory T cells (Treg) (Liu et al., 2026a). Butyrate from gut microbiota can boost anti-tumor immunity by training intestinal macrophages (Liu et al., 2026b). Mitochondrial DNA sensing can activate via cGAS-STING and synergistically remodel the tumor immune microenvironment with ferroptosis (Liu et al., 2026c). At the same time, explainable spatial artificial intelligence (AI) has been used to analyze tumor-immune interactions and predict immunotherapy outcomes (Liu et al., 2026d). Multimodal foundational models can predict the immunogenicity of new antigens and vaccine effectiveness (Liu et al., 2026e). AI integration of multi-omics data is also used for predicting the effectiveness of immunotherapy and optimizing combination strategies (Liu, 2026a). The composition, dynamic evolution, and clinical significance of the tumor microenvironment are also systematically explained (Liu, 2026b). However, these studies haven't really dug into the key role of the lactate metabolism-histone lactylation axis in $CD8^+$ T cell exhaustion, nor have they systematically linked it to the new immune therapy strategies mentioned above.

The contribution of this study lies in systematically analyzing the lactate metabolism

characteristics of tumor-infiltrating $CD8^+$ T cells and clarifying the role of lactate metabolism reprogramming mediated by LDHA/MCT1/4 in T cell exhaustion; revealing a new mechanism where histone lactylation acts as a metabolism-epigenetic bridge to regulate the expression of exhaustion-related genes; and evaluating the synergistic anti-tumor effects of targeting lactate metabolism combined with anti-PD-1 therapy. The findings will provide new metabolic-epigenetic intervention targets for immunotherapy in solid tumors.

3. Materials and Methods

3.1. Cell lines and culture

Mouse melanoma cell line B16-OVA, mouse colon cancer cell line MC38, and human embryonic kidney cell line HEK293T purchased from the American Typical Culture Conservation Center (ATCC) or the National Experimental Cell Resource Sharing Platform. B16-OVA cells were cultured in DMEM high-sugar medium containing 10% fetal bovine serum (FBS), 1% penicillin/streptomycin, and 400 μg/mL G418; MC38 cells were cultured in RPMI-1640 medium containing 10% FBS and 1% penicillin/streptomycin; HEK293T cells were cultured in DMEM medium containing 10% FBS. All cells were cultured in 37°C, 5% CO_2, saturated humidity incubators, and passaged every 2-3 days. Before the experiment, mycoplasma detection kits were used to confirm the absence of mycoplasma contamination, and cell identity was confirmed by STR identification. All experiments used logarithmic anagen cells, with passage times not exceeding 20 generations.

3.2. Experimental animals

Female C57BL/6J wild-type mice, aged 6-8 weeks, were purchased from Beijing Vital River Laboratory Animal Technology Co., Ltd. or Jackson Laboratory. $CD8^+$ T cell-specific Ldha knockout mice (Cd8-Cre; Ldhafl/fl), MCT1 knockout mice (Cd8-Cre; Slc16a1fl/fl), and MCT4 knockout mice (Cd8-Cre; Slc16a3fl/fl) were generated by crossing Cd8-Cre mice with the corresponding floxed mice. The controls were Ldhafl/fl, Slc16a1fl/fl, or Slc16a3fl/fl mice. All mice were housed in SPF-grade barrier conditions, with free access to food and water, under a 12-hour light-dark cycle.

3.3. Tumor models and experimental design

B16-OVA cells (1×10^6/100 μL PBS) or MC38 cells (5×10^5/100 μL PBS) were subcutaneously injected into the right back of mice. When the tumor volume reached about 50-100 mm^3, the mice were randomly divided into the following groups: solvent control, LDHA inhibitor, MCT1/4 inhibitor, anti-PD-1, and combination therapy. The LDHA inhibitor GNE-140 (40 mg/kg, intraperitoneal injection, once daily) or the MCT1/4 inhibitor AZD3965 (100 mg/kg, oral gavage, twice daily) was administered alone or together with anti-PD-1 antibody (clone RMP1-14, 200 μg per mouse,

intraperitoneal injection, every 3 days); the control group received an equal volume of solvent or isotype control IgG. Tumor length and width were measured every 2-3 days with a caliper, and tumor volume was calculated using the formula V = length × width² / 2. At the endpoint, mice were sacrificed, and tumor tissues, spleen, draining lymph nodes, and peripheral blood were collected for further analysis. To verify $CD8^+$ T cell dependence, some mice were intraperitoneally injected with anti-CD8α depleting antibody (clone 2.43, 200 μg per mouse) 1 day before tumor injection and on days 1 and 3 after injection.

3.4. Single-cell RNA sequencing

Fresh tumor tissue was collected and digested at 37°C for 30 minutes with collagenase IV (1 mg/mL), DNase I (100 μg/mL), and hyaluronidase (0.5 mg/mL) to prepare a single-cell suspension. $CD45^+CD3^+CD8^+$ T cells were isolated using magnetic bead sorting or flow cytometry, with cell viability over 90%. Single-cell libraries were constructed following the 10x Genomics Chromium 3' v3.1 kit instructions and sequenced on the Illumina NovaSeq 6000 platform. Raw data were aligned to the mouse reference genome mm10 using Cell Ranger 7.0 to generate gene expression matrices. Quality control was performed using Seurat 4.0: cells with nFeature_RNA 200-5000 and percent.mt <10% were retained, and doublets were removed using DoubletFinder. Batch correction was done with Harmony, UMAP was used for dimensionality reduction and clustering, and cell subpopulations were identified with FindClusters. Differentially expressed genes were screened using FindMarkers, followed by GO and KEGG enrichment analyses. Pseudotime analysis was performed using Monocle3, transcriptional regulatory networks were analyzed with SCENIC, and AddModuleScore was used to evaluate gene set scores related to lactate metabolism and T cell exhaustion.

3.5. Metabolomics analysis

Collect tumor tissues or sorted $CD8^+$ T cells, and extract metabolites using cold methanol/water (4:1, v/v). After centrifugation to remove proteins, use the supernatant for LC-MS/MS analysis. Detect metabolites like lactate, pyruvate, TCA cycle intermediates, amino acids, and nucleotides using an Agilent 1290 Infinity UPLC system coupled with a 6470 triple quadrupole mass spectrometer or an Orbitrap high-resolution mass spectrometer. Process the data with MetaboAnalyst 5.0, and screen for differential metabolites using VIP >1, fold change (FC) >1.5, and FDR <0.05. QC samples were included for all samples to ensure data stability.

3.6. Flow cytometry

Tumor-infiltrating lymphocytes were prepared as described earlier. For cell surface staining, the following antibodies were used: CD45-BV510, CD3-BV650, CD8-APC-Cy7, PD-1-BV421, TIM-3-PE, LAG-3-APC, CD44-FITC, CD62L-PE-Cy7. For intracellular staining, a

fixation/permeabilization kit was used, with antibodies including IFN-γ-PE-Cy7, TNF-α-BV421, Granzyme B-FITC, TOX-AF647, Ki-67-BV605. Nuclear transcription factor staining was done using FoxP3/transcription factor fixation and permeabilization buffer. Mitochondrial function was assessed with MitoTracker Green, MitoSOX, and TMRM. Lactate uptake was measured using fluorescent lactate analogs or 2-NBDG as a control. All samples were acquired on BD FACSCanto II or CytoFLEX flow cytometers and analyzed with FlowJo 10.8 software. Cytokine secretion was detected using ELISA or CBA.

3.7. Immunohistochemistry and immunofluorescence

Tumor tissues were fixed in 4% paraformaldehyde and embedded in paraffin, then cut into 4 μm sections. For immunohistochemistry, antigen retrieval was done using citrate buffer (pH 6.0) or EDTA buffer (pH 9.0), endogenous peroxidase was blocked with 3% H_2O_2, and 5% BSA was used for blocking. Primary antibodies included anti-CD8, anti-LDHA, anti-MCT1, anti-MCT4, anti-H3K18la, and anti-pan-Kla, and were incubated overnight at 4°C. The next day, HRP-conjugated secondary antibodies were added, DAB was used for color development, and hematoxylin was used for counterstaining. For immunofluorescence, Alexa Fluor 488 or 594-labeled secondary antibodies were used, DAPI was used to stain nuclei, and images were captured with a confocal microscope. ImageJ or HALO software was used for quantitative analysis, and results were expressed as H-score or percentage of positive cells.

3.8. Real-time quantitative PCR and western blot

Total RNA was extracted using Trizol reagent, reverse-transcribed to synthesize cDNA, and real-time quantitative PCR was performed using the SYBR Green method. The primer sequences targeted Pdcd1, Havcr2, Lag3, Tox, Nr4a1, Ifng, Tnf, Gzmb, Ldha, Slc16a1, Slc16a3, and β-actin, and relative expression levels were calculated using the $2^{-\Delta\Delta Ct}$ method. For Western blot, cells were lysed with RIPA buffer, protein concentration was measured using the BCA method, separated by SDS-PAGE, and transferred to a PVDF membrane. After blocking with 5% BSA, primary antibodies were incubated overnight at 4°C. The primary antibodies included anti-LDHA, anti-MCT1, anti-MCT4, anti-H3K18la, anti-H4K12la, anti-pan-Kla, anti-β-actin, and anti-histone H3. The next day, HRP-conjugated secondary antibodies were added, ECL chemiluminescence was used for detection, and band intensity was quantified using ImageLab or ImageJ.

3.9. Lactate testing and seahorse metabolic analysis

Lactate levels in the culture supernatant and inside the cells were measured using a lactate assay kit (colorimetric or fluorescent), following the instructions carefully. Cell glycolysis and mitochondrial respiration were detected using a Seahorse XFe96 extracellular flux analyzer. Cells were seeded in

XFe96 plates, and the next day the assay medium was replaced. Oligomycin, FCCP, rotenone/antimycin A, and 2-DG were injected in sequence to measure extracellular acidification rate (ECAR) and oxygen consumption rate (OCR). Parameters like basal glycolysis, maximal glycolysis, basal respiration, maximal respiration, and ATP production were calculated.

3.10. Detection of histone lactylation and ChIP-qPCR

Histone lactylation levels were detected by Western blot using anti-H3K18la, anti-H4K12la, and anti-pan-Kla antibodies. For chromatin immunoprecipitation (ChIP) experiments, cells were crosslinked with 1% formaldehyde for 10 minutes, quenched with glycine, and sonicated to break the chromatin into 200–500 bp fragments. Anti-H3K18la antibody or control IgG was added and incubated overnight at 4°C, followed by the addition of protein A/G magnetic beads. After washing, elution, reverse crosslinking, and DNA purification, qPCR was used to detect enrichment at the promoters of genes like Pdcd1, Havcr2, Lag3, and Tox. The results were expressed as a percentage of input DNA or as relative enrichment.

3.11. PD-1 combination therapy experiment

In the B16-OVA and MC38 tumor-bearing mouse models, once the tumors reached 50-100 mm^3, the mice were randomly divided into groups and given either a solvent, an LDHA inhibitor, an MCT1/4 inhibitor, an anti-PD-1 antibody, or a combination treatment. The anti-PD-1 antibody (clone RMP1-14) was administered at 200 μg per mouse intraperitoneally, once every 3 days for a total of 4 doses. Tumor volume and body weight were monitored every 2–3 days, and tumor growth curves and Kaplan-Meier survival curves were plotted. At the endpoint, tumor tissues were collected to analyze $CD8^+$ T cell infiltration by flow cytometry, assess exhaustion marker expression and effector cytokine secretion, and perform immunohistochemistry to examine $CD8^+$ T cell infiltration and H3K18la levels.

3.12. Data analysis and statistics

All experimental data were statistically analyzed using GraphPad Prism 9 and R 4.2. Data are presented as mean ± SEM. Normality was tested with the Shapiro-Wilk test, and homogeneity of variance was tested with the F test. Comparisons between two groups were done using independent-sample t-tests or Mann-Whitney U tests; comparisons among multiple groups were done using one-way or two-way ANOVA, with post hoc tests using Tukey or Bonferroni corrections. Survival analysis was done using the Kaplan-Meier method and log-rank test. Single-cell sequencing data were analyzed using Seurat, Monocle3, and SCENIC; metabolomics data were analyzed with MetaboAnalyst 5.0. All tests were two-sided, and $P < 0.05$ was considered statistically significant. Each group had n = 5-6 samples, and all experiments were independently repeated at least three times. Animal experiments used random grouping, and data collection and analysis were blinded. Samples

were excluded if tumors did not form, if animals died, or if data were missing.

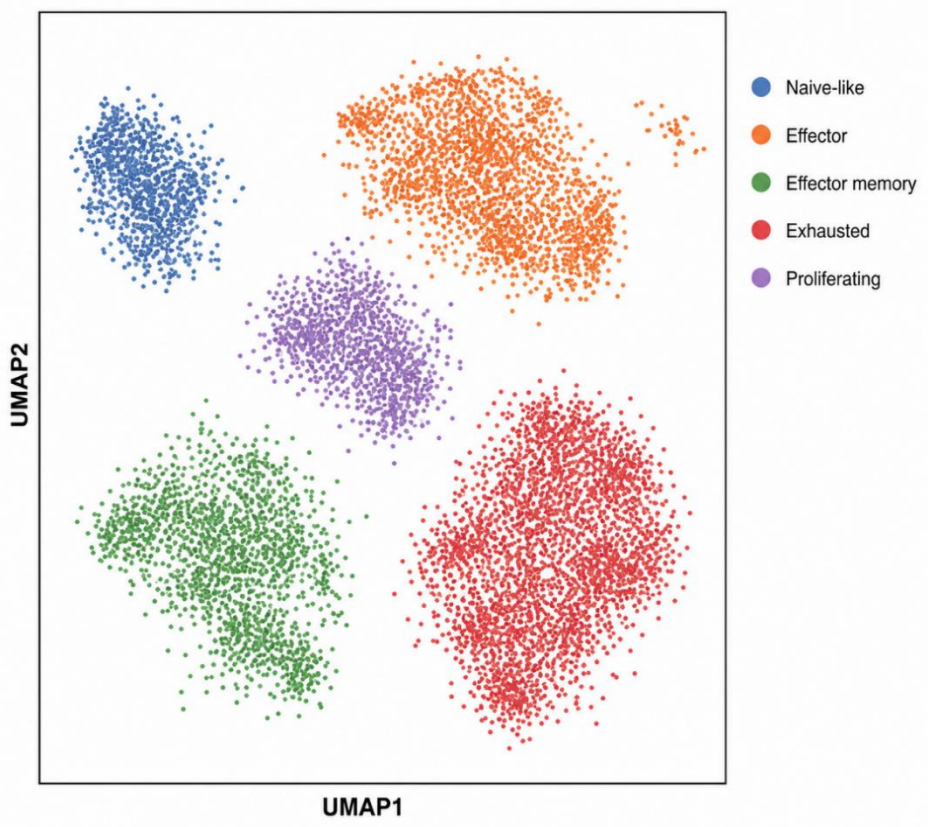
4. Results

4.1. Tumor-infiltrating CD8⁺ T cells show lactate metabolism reprogramming and exhaustion features

To explore the heterogeneity of CD8⁺ T cells in the tumor microenvironment, we performed single-cell RNA sequencing on tumor-infiltrating CD8⁺ T cells from B16-OVA and MC38 tumor-bearing mice. UMAP clustering identified five CD8⁺ T cell subpopulations: naive-like, effector, effector memory, exhausted, and proliferating (Figure 1A). Among these, the exhausted subpopulation was the largest, making up 41.6%, and it highly expressed Pdcd1, Havcr2, Lag3, and Tox, with both exhaustion and lactate metabolism scores significantly increased (Table 1). Metabolomics analysis showed that, compared to control CD8⁺ T cells, tumor-infiltrating CD8⁺ T cells had a 2.91-fold increase in lactate and a 1.43-fold increase in pyruvate, while citrate, α-ketoglutarate, and ATP levels decreased to 0.68, 0.74, and 0.61 times, respectively (Table 2). Flow cytometry further confirmed that LDHA, MCT1, and MCT4 protein expression was upregulated in tumor-infiltrating CD8⁺ T cells, enhancing their lactate uptake ability (Figures 1B-C, Table 1B-C).

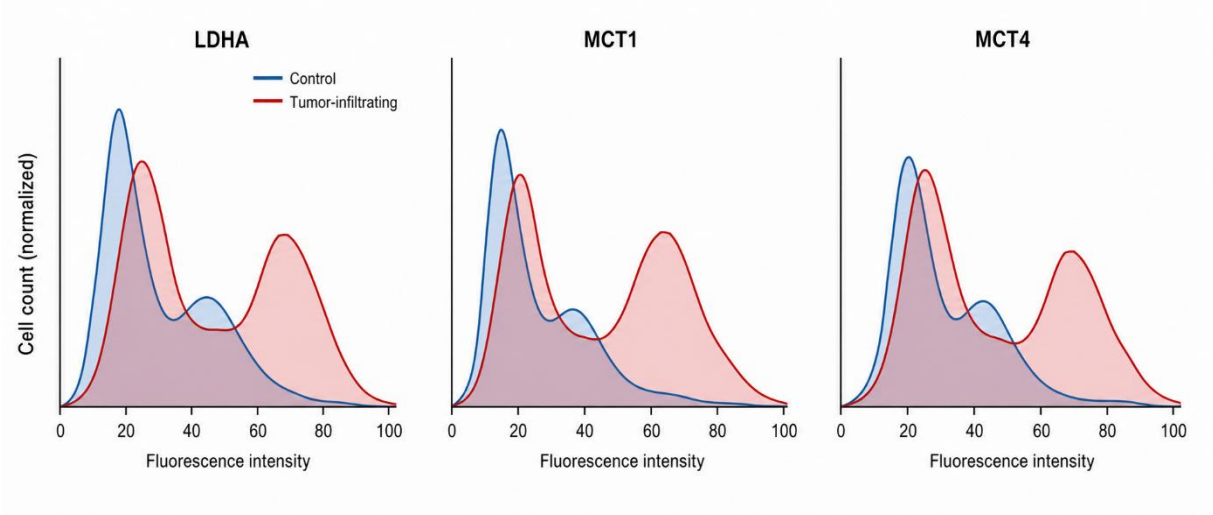
Figure 1

A: CD8⁺ T cell UMAP clustering map



B: Representative flow cytometry histograms of LDHA, MCT1, and MCT4

Global Health Care
WISDOM ACADEMIC https://doi.org/10.63808/ghc.v2i1.535 Volume 2 , Issue 1



C: Quantification of lactate uptake fluorescence intensity

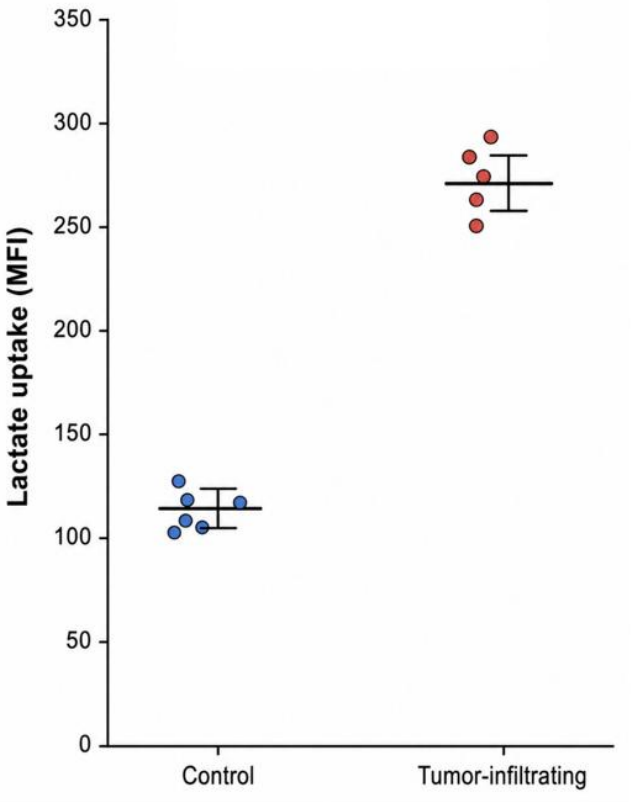


Table 1

Characteristics of CD8⁺ T cell subsets identified by single-cell RNA sequencing

subgroup	Proportion (%)	Key gene	Fatigue Score	Lactic Acid Metabolism Score
Naive-like	8.7	Sell, Ccr7, Tcf7	0.12	0.08
Effector	22.4	Ifng, Gzmb, Prf1	0.35	0.42
Effector memory	15.9	Cd44, Tcf7, Il7r	0.28	0.31
Exhausted	41.6	Pdcd1, Havcr2,	0.87	0.79

		Lag3, Tox		
Proliferating	11.4	Mki67, Stmn1	0.44	0.53

Table 2

Relative abundance of differential metabolites in tumor-infiltrating CD8⁺ T cells

Metabolite	control group	Tumor-infiltrating CD8⁺ T cells	P-value
Lactic acid	1.00 ± 0.08	2.91 ± 0.24	<0.001
Pyruvic acid	1.00 ± 0.09	1.43 ± 0.15	0.012
citric acid	1.00 ± 0.07	0.68 ± 0.06	0.006
α-ketoglutaric acid	1.00 ± 0.11	0.74 ± 0.08	0.021
ATP	1.00 ± 0.06	0.61 ± 0.05	0.003
NAD^+/NADH	1.00 ± 0.10	0.72 ± 0.09	0.018

Table 1B

Representative flow cytometry histograms of LDHA, MCT1, and MCT4

Curve	Amplitude	mean mu	Standard deviation sigma
LDHA Control	1.0	18	7.5
LDHA Control	0.35	42	11
LDHA Tumor	0.85	24	8.2
LDHA Tumor	0.90	58	12.5
MCT1 Control	1.0	16	7.0
MCT1 Control	0.28	38	10
MCT1 Tumor	0.80	22	8.0
MCT1 Tumor	0.95	55	13
MCT4 Control	1.0	20	8.0
MCT4 Control	0.30	44	12
MCT4 Tumor	0.78	26	8.5
MCT4 Tumor	0.88	60	13.5

Table 1C

Quantification of lactate uptake fluorescence intensity

Group	Rep1	Rep2	Rep3	Rep4	Rep5	Rep6
Control	104.2	118.6	109.5	126.3	101.8	115.4

Tumor-infiltrating	254.6	281.3	263.8	292.1	248.9	272.4

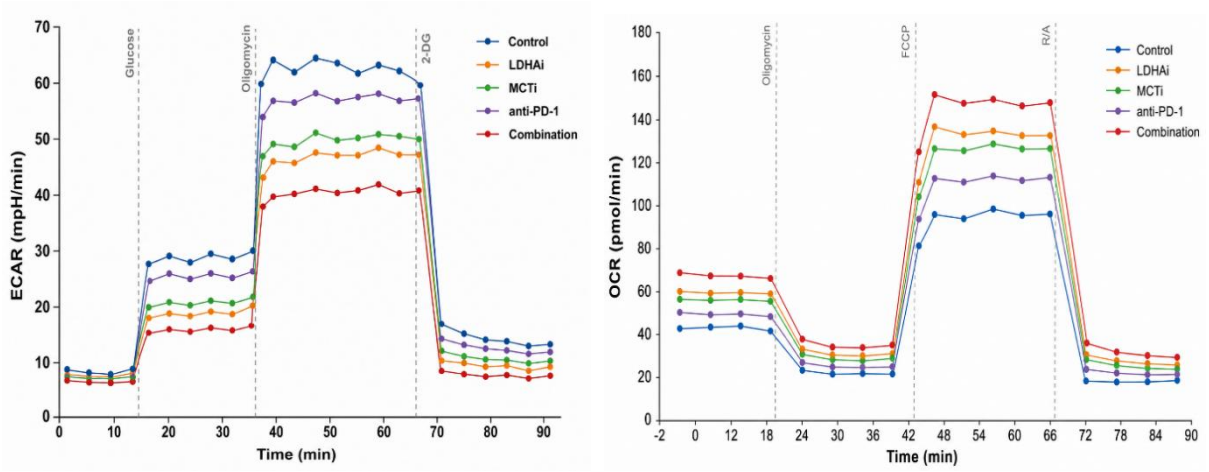
4.2. Inhibiting LDHA or MCT1/4 restores mitochondrial function and oxidative phosphorylation in CD8⁺ T cells

To figure out how lactate metabolism affects CD8⁺ T cell metabolic function, we treated tumor-infiltrating CD8⁺ T cells with the LDHA inhibitor GNE-140 or the MCT1/4 inhibitor AZD3965. Seahorse analysis showed that after inhibiting LDHA or MCT1/4, the basal and maximal ECAR went down, while basal OCR, maximal OCR, and ATP production went up significantly (Table 3, Figures 2A-B, Table 2A-B). Staining with MitoTracker Green and TMRM showed that mitochondrial mass and membrane potential recovered, and the percentage of MitoSOX-positive cells decreased after LDHA or MCT1/4 inhibition (Figures 2C-D, Table 2C-D). These results suggest that targeting lactate metabolism can reverse mitochondrial dysfunction in tumor-infiltrating CD8⁺ T cells.

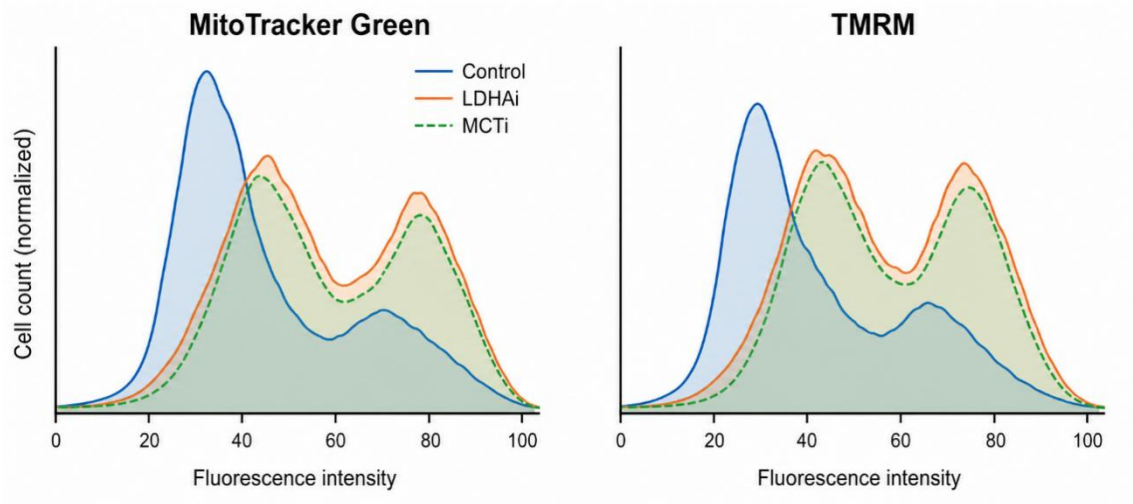
Figure 2

A: Lactate metabolism intervention restores CD8⁺ T cell mitochondrial function - ECAR curve

B: Lactate metabolism intervention restores CD8⁺ T cell mitochondrial function - OCR curve



C: Representative flow cytometry plots of MitoTracker Green and TMRM



D: Quantification of MitoSOX-positive cell proportion

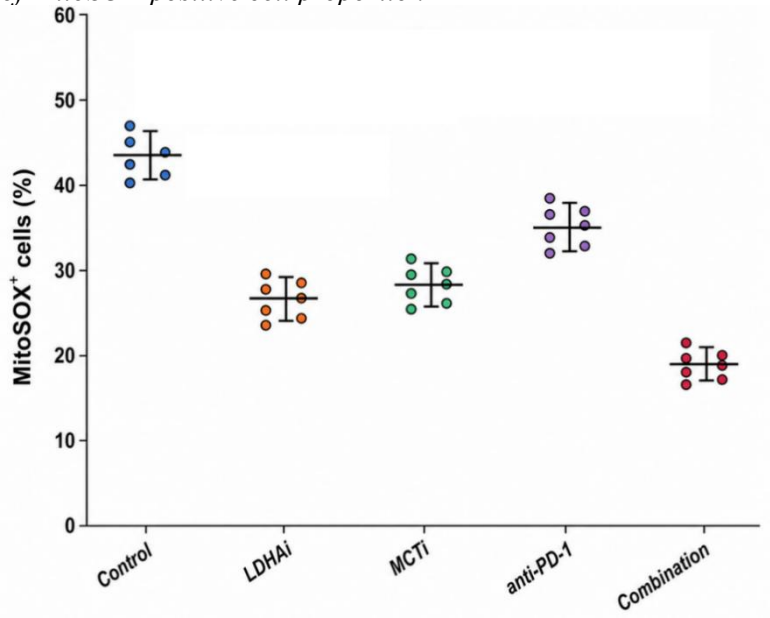


Table 2

A: Lactate metabolism intervention restores CD8⁺ T cell mitochondrial function - ECAR curve

Group	base	glyco	max	final
Control	8.2	27.5	64.3	14.2
LDHAi	7.8	19.1	47.6	10.8
MCTi	8.0	20.3	49.8	11.6
anti-PD-1	8.1	24.2	56.9	12.9
Combination	7.6	15.8	40.7	8.7

B: Lactate metabolism intervention restores CD8⁺ T cell mitochondrial function - OCR curve

Group	base	oligo	fccp	ra
Control	42.3	21.6	96.8	18.4
LDHAi	58.7	30.2	131.4	25.6
MCTi	56.4	29.4	127.9	24.8
anti-PD-1	49.6	25.1	111.7	21.3
Combination	66.9	34.8	148.2	29.5

C: Representative flow cytometry plots of MitoTracker Green and TMRM

Curve	Amplitude	mean mu	Standard deviation sigma
MitoTracker Green Control	1.0	34	10
MitoTracker Green Control	0.35	62	14

MitoTracker Green LDHAi	0.85	44	11
MitoTracker Green LDHAi	0.70	72	13
MitoTracker Green MCTi	0.88	42	10.5
MitoTracker Green MCTi	0.72	70	12.8
TMRM Control	1.0	28	9
TMRM Control	0.30	55	13
TMRM LDHAi	0.80	40	10
TMRM LDHAi	0.80	68	14
TMRM MCTi	0.82	38	10
TMRM MCTi	0.78	66	13.5

D: Quantification of MitoSOX-positive cells

Group	Rep1	Rep2	Rep3	Rep4	Rep5	Rep6
Control	42.6	46.1	39.8	44.3	47.5	41.2
LDHAi	27.4	24.8	29.6	26.1	23.5	28.2
MCTi	28.9	26.3	30.7	27.5	25.1	29.4
anti-PD-1	34.7	37.2	32.5	35.8	38.4	33.1
Combination	18.6	16.9	21.3	19.4	17.2	20.5

Table 3

$CD8^+$ T cell metabolic parameters

Group	Basic ECAR	Max ECAR	Basic OCR	Max OCR	ATP production
Control	28.4 ± 2.1	65.7 ± 4.8	42.6 ± 3.5	98.3 ± 7.2	18.7 ± 1.6
LDHAi	19.6 ± 1.8	48.2 ± 3.9	58.9 ± 4.2	132.5 ± 9.1	27.4 ± 2.2
MCTi	20.8 ± 1.9	50.5 ± 4.1	56.3 ± 4.0	128.7 ± 8.8	26.1 ± 2.1
anti-PD-1	24.7 ± 2.0	57.3 ± 4.4	49.8 ± 3.8	112.4 ± 8.0	22.3 ± 1.9
Combination	16.3 ± 1.5	41.6 ± 3.4	67.2 ± 4.8	148.9± 10.3	31.8 ± 2.5

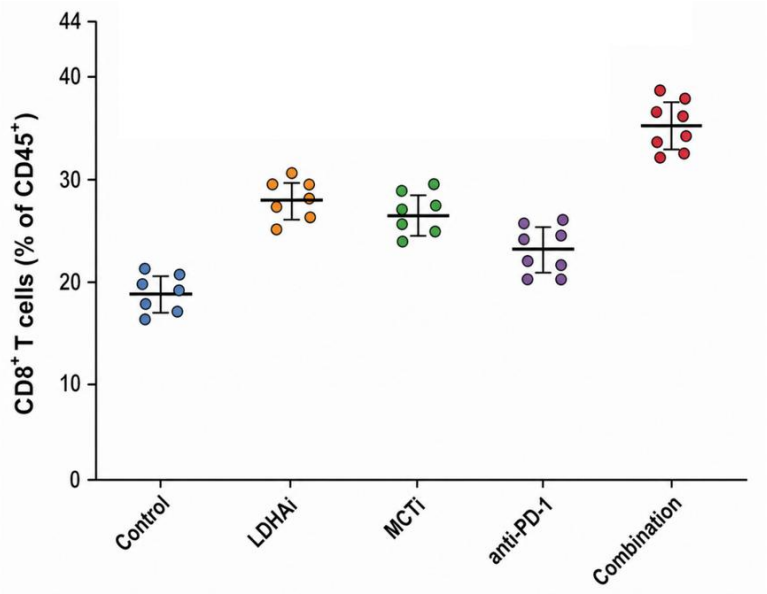
4.3. Lactic acid metabolism reprogramming reverses $CD8^+$ T cell exhaustion and boosts effector function

Flow cytometry analysis showed that after inhibiting LDHA or MCT1/4, the proportion of tumor-infiltrating $CD8^+$ T cells significantly increased, and the proportions of IFN-γ^+, TNF-α^+, and Granzyme B^+ cells went up, while PD-1^+, TIM-3^+, LAG-3^+, and TOX^+ cells went down (Table 3A-E,

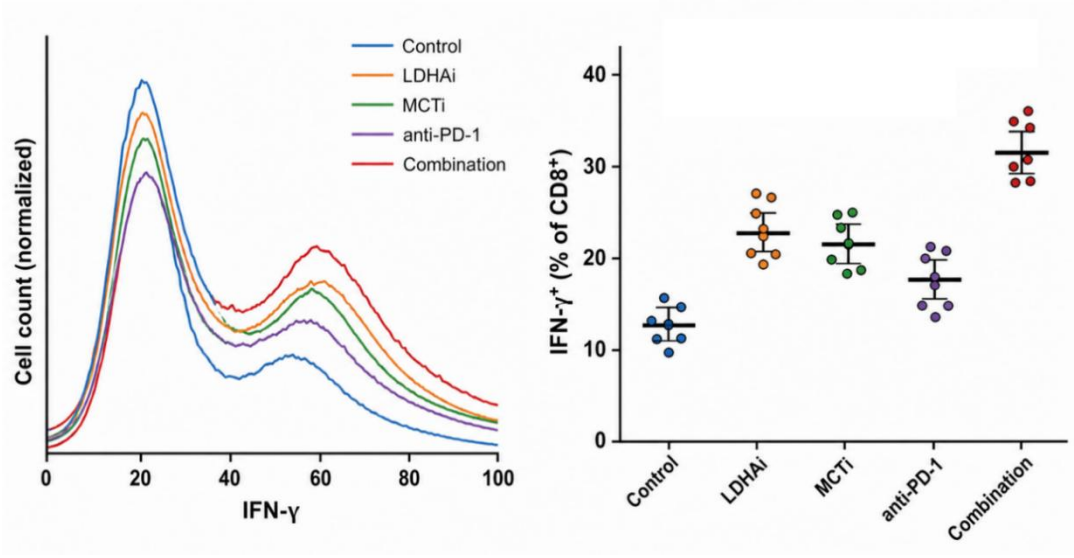
Figures 3A-E). These effects were further enhanced when combined with anti-PD-1 treatment. RT-qPCR results matched the flow cytometry data: after inhibiting LDHA or MCT1/4, Ifng, Tnf, and Gzmb mRNA levels went up, while Pdcd1, Havcr2, Lag3, and Tox mRNA levels went down (Figure 3F, Table 3F).

Figure 3

A: Proportion of CD8⁺ T cell infiltration

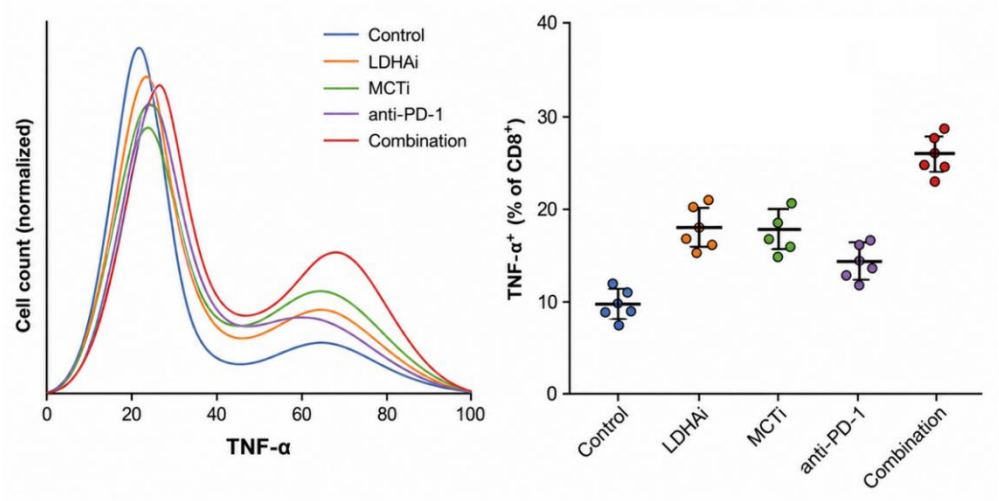


B: Representative flow cytometry plot and quantification of IFN-γ+

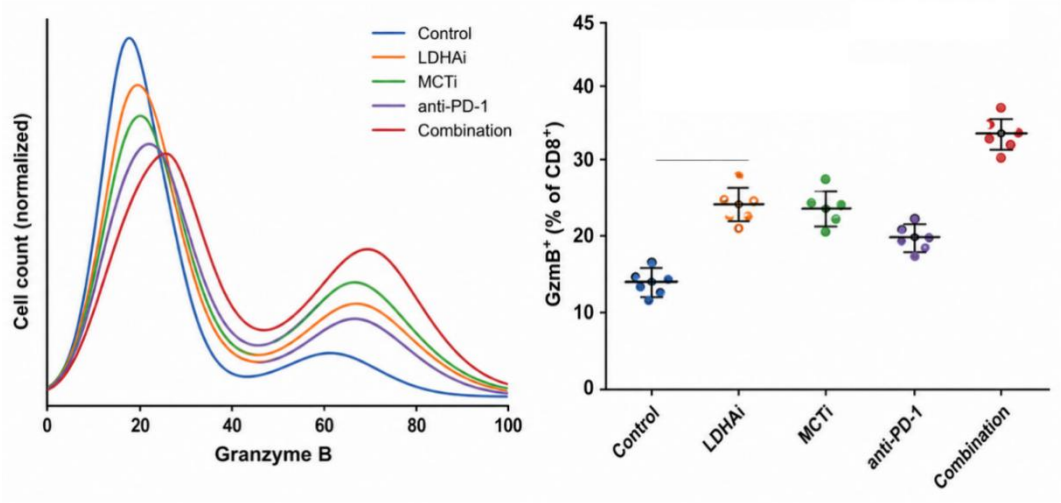


C: Representative flow cytometry plot and quantification of TNF-α+

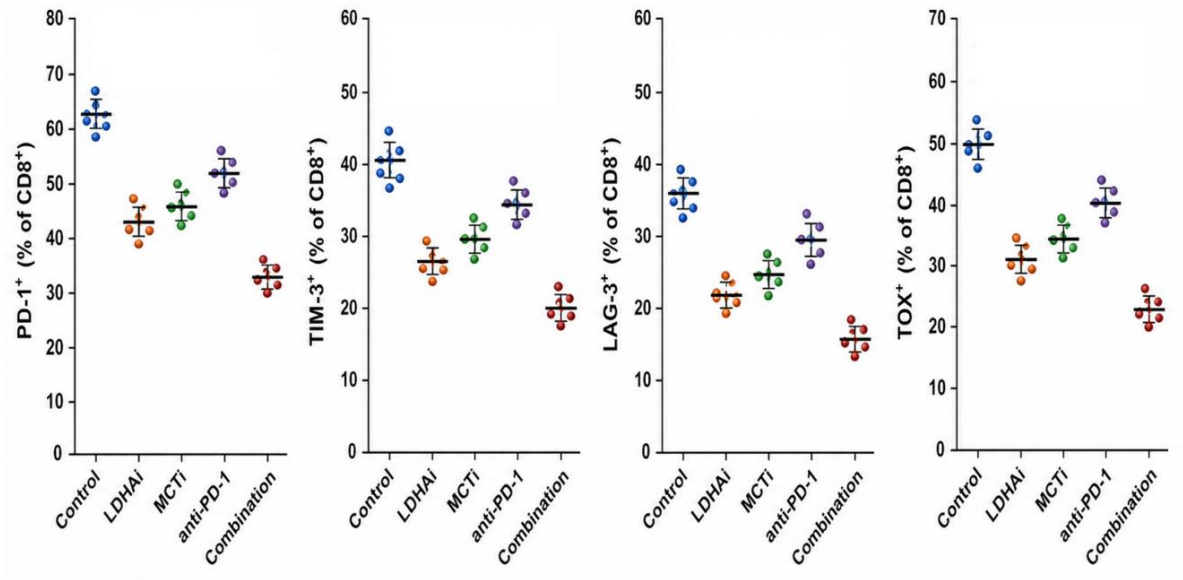
Global Health Care
WISDOM ACADEMIC https://doi.org/10.63808/ghc.v2i1.535 Volume 2 , Issue 1



D: Representative flow cytometry plot and quantification of Granzyme B+



E: Quantification of PD-1, TIM-3, LAG-3, TOX expression



F: Relative mRNA expression of exhaustion- and effector-related genes

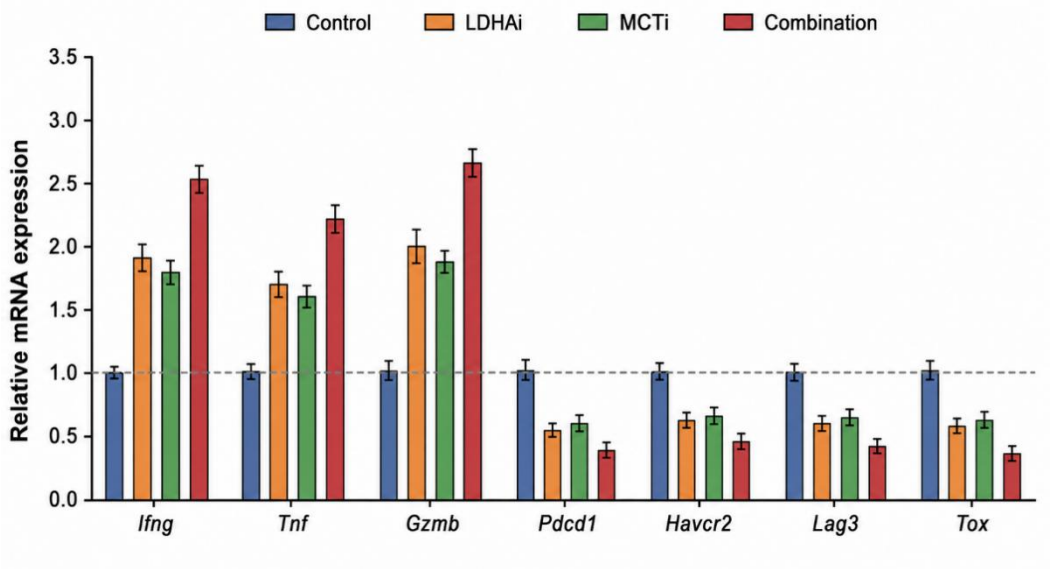


Table 3

A: Proportion of CD8⁺ T cell infiltration

Group	CD8⁺ T cell percentage (%)
Control	18.4 ± 2.1
LDHAi	27.9 ± 2.6
MCTi	26.5 ± 2.4
anti-PD-1	22.3 ± 2.2
Combination	34.6 ± 3.0

B: Representative flow cytometry plot and quantification of IFN-γ+

Group	IFN-γ⁺（%）
Control	12.7 ± 1.8
LDHAi	23.4 ± 2.2
MCTi	21.8 ± 2.0
anti-PD-1	17.5 ± 1.9
Combination	31.2 ± 2.7

C: Representative flow cytometry plot and quantification of TNF-α+

Group	TNF-α⁺（%）
Control	9.5 ± 1.3
LDHAi	18.6 ± 1.9
MCTi	17.2 ± 1.7

anti-PD-1	13.8 ± 1.5
Combination	25.9 ± 2.3

D: Representative flow cytometry plot and quantification of Granzyme B+

Group	GzmB⁺（%）
Control	14.2 ± 1.5
LDHAi	25.7 ± 2.3
MCTi	24.1 ± 2.1
anti-PD-1	19.6 ± 1.8
Combination	33.5 ± 2.8

E: Quantification of PD-1, TIM-3, LAG-3, TOX expression

Group	PD-1⁺（%）	TIM-3⁺（%）	LAG-3⁺（%）	TOX⁺（%）
Control	62.3 ± 4.5	41.2 ± 3.7	35.8 ± 3.1	48.6 ± 4.1
LDHAi	43.1 ± 3.8	27.5 ± 2.9	22.4 ± 2.5	31.5 ± 3.0
MCTi	45.7 ± 4.0	29.8 ± 3.0	24.1 ± 2.6	33.8 ± 3.2
anti-PD-1	51.6 ± 4.2	33.4 ± 3.3	28.7 ± 2.8	39.4 ± 3.5
Combination	32.8 ± 3.1	19.6 ± 2.4	15.3 ± 1.9	22.7 ± 2.4

F: Relative mRNA expression of exhaustion- and effector-related genes

Gene	Group	Rep1	Rep2	Rep3	Rep4	Rep5	Rep6
Ifng	Control	1.00	0.92	1.08	0.96	1.04	0.98
Ifng	LDHAi	1.86	2.04	1.72	1.94	1.81	2.11
Ifng	MCTi	1.78	1.92	1.65	1.85	1.73	1.97
Ifng	Combination	2.43	2.68	2.31	2.57	2.39	2.71
Tnf	Control	1.00	1.06	0.94	1.03	0.97	1.05
Tnf	LDHAi	1.65	1.78	1.55	1.69	1.58	1.83
Tnf	MCTi	1.55	1.72	1.44	1.62	1.52	1.79
Tnf	Combination	2.14	2.36	2.03	2.27	2.08	2.41
Gzmb	Control	1.00	0.95	1.07	0.98	1.03	1.01
Gzmb	LDHAi	1.92	2.11	1.81	2.04	1.88	2.18
Gzmb	MCTi	1.81	1.99	1.71	1.93	1.78	2.06
Gzmb	Combination	2.57	2.81	2.43	2.72	2.49	2.86

Pdcd1	Control	1.00	1.04	0.96	1.02	0.98	1.03
Pdcd1	LDHAi	0.54	0.49	0.58	0.52	0.46	0.58
Pdcd1	MCTi	0.56	0.52	0.65	0.57	0.53	0.62
Pdcd1	Combination	0.38	0.32	0.44	0.35	0.30	0.41
Havcr2	Control	1.00	0.97	1.05	0.99	1.02	0.98
Havcr2	LDHAi	0.62	0.56	0.65	0.59	0.54	0.66
Havcr2	MCTi	0.66	0.62	0.73	0.69	0.58	0.70
Havcr2	Combination	0.44	0.38	0.51	0.41	0.36	0.48
Lag3	Control	1.00	1.03	0.95	1.01	0.97	1.04
Lag3	LDHAi	0.57	0.53	0.69	0.56	0.57	0.63
Lag3	MCTi	0.63	0.70	0.60	0.60	0.55	0.67
Lag3	Combination	0.41	0.35	0.48	0.38	0.33	0.45
Tox	Control	1.00	0.98	1.06	1.00	1.03	0.97
Tox	LDHAi	0.57	0.51	0.64	0.54	0.49	0.61
Tox	MCTi	0.61	0.57	0.65	0.56	0.59	0.68
Tox	Combination	0.36	0.30	0.43	0.33	0.28	0.40

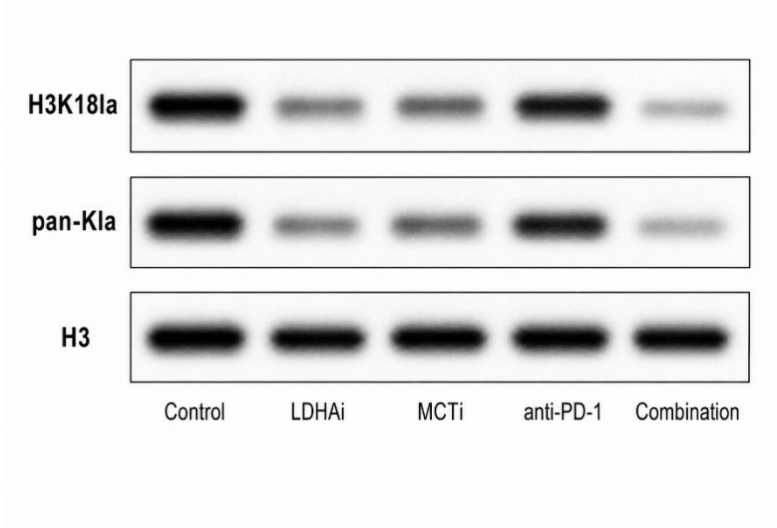
4.4. Histone lactylation mediates the expression of exhaustion-related genes

Western blot showed that H3K18la and pan-Kla levels were elevated in tumor-infiltrating $CD8^+$ T cells, but significantly decreased after inhibiting LDHA or MCT1/4 (Fig. 4A-B, Table 4A-B). ChIP-qPCR analysis showed that the H3K18la antibody was significantly enriched at the promoters of Pdcd1, Havcr2, Lag3, and Tox, but not at the Ifng promoter (Table 4C, Fig. 4C). After combining with anti-PD-1 treatment, H3K18la enrichment at the promoters of exhaustion-related genes decreased even further (Fig. 4D). These results suggest that lactate regulates the transcription of exhaustion-related genes through histone lactylation.

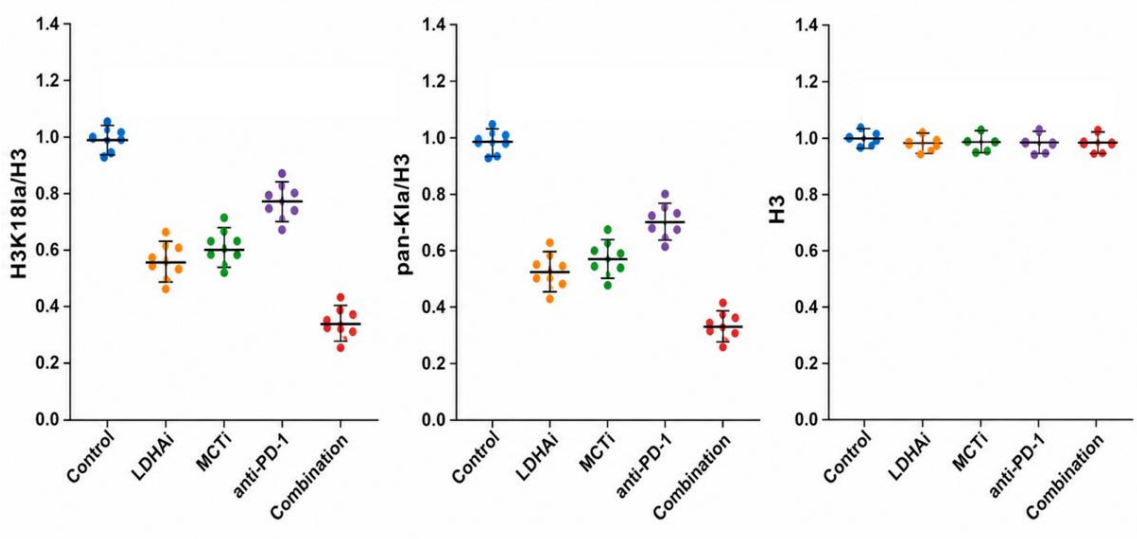
Figure 4

A: Representative Western blot of H3K18la and pan-Kla

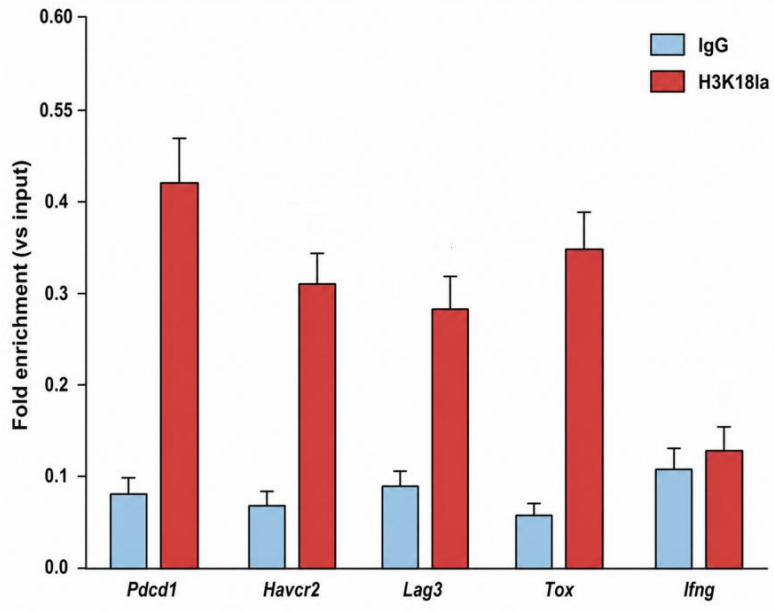
https://doi.org/10.63808/ghc.v2i1.535 Volume 2 , Issue 1



B: Quantification of relative protein levels



C: ChIP-qPCR enrichment fold



D: Changes in H3K18la enrichment after combined treatment

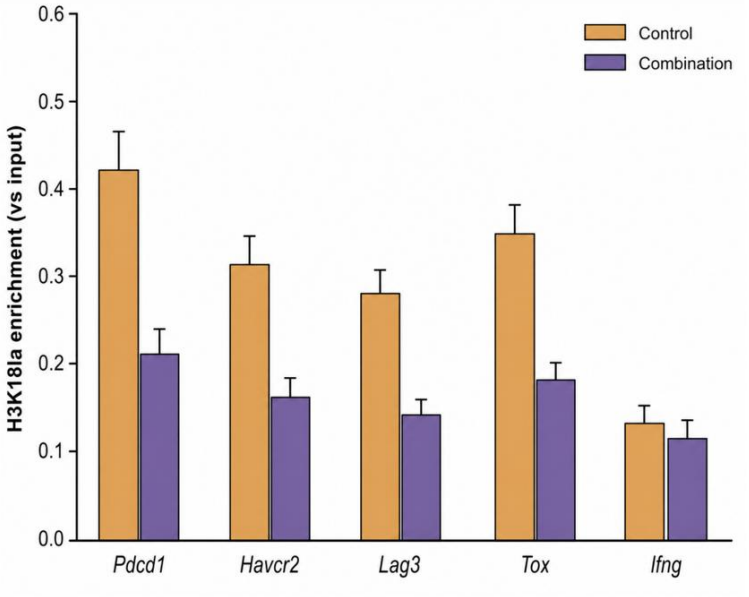


Table 4

A: Representative Western blot of H3K18la and pan-Kla

protein	Control	LDHAi	MCTi	anti-PD-1	Combination
H3K18la	0.86	0.52	0.55	0.71	0.34
pan-Kla	0.78	0.49	0.52	0.64	0.31
H3	0.82	0.80	0.83	0.81	0.79

B: Quantification of relative protein levels

Indicator	Group	Rep1	Rep2	Rep3	Rep4	Rep5	Rep6
H3K18la/H3	Control	1.00	1.06	0.94	1.03	0.97	1.05
H3K18la/H3	LDHAi	0.57	0.51	0.63	0.55	0.49	0.61
H3K18la/H3	MCTi	0.60	0.54	0.66	0.58	0.52	0.64
H3K18la/H3	anti-PD-1	0.78	0.72	0.84	0.76	0.70	0.82
H3K18la/H3	Combination	0.36	0.30	0.42	0.34	0.28	0.40
pan-Kla/H3	Control	1.00	0.97	1.05	1.01	0.99	1.03
pan-Kla/H3	LDHAi	0.53	0.47	0.59	0.51	0.45	0.57
pan-Kla/H3	MCTi	0.56	0.50	0.62	0.54	0.48	0.60
pan-Kla/H3	anti-PD-1	0.70	0.64	0.76	0.68	0.62	0.74
pan-Kla/H3	Combination	0.33	0.27	0.39	0.31	0.25	0.37
H3	Control	1.00	1.02	0.98	1.01	0.99	1.00

H3	LDHAi	0.98	1.00	0.96	0.99	0.97	0.99
H3	MCTi	1.01	0.99	1.03	1.00	0.98	1.02
H3	anti-PD-1	0.99	1.01	0.97	1.00	0.98	1.01
H3	Combination	1.00	0.98	1.02	0.99	0.97	1.01

C: ChIP-qPCR enrichment of H3K18la at promoters of exhaustion-related genes

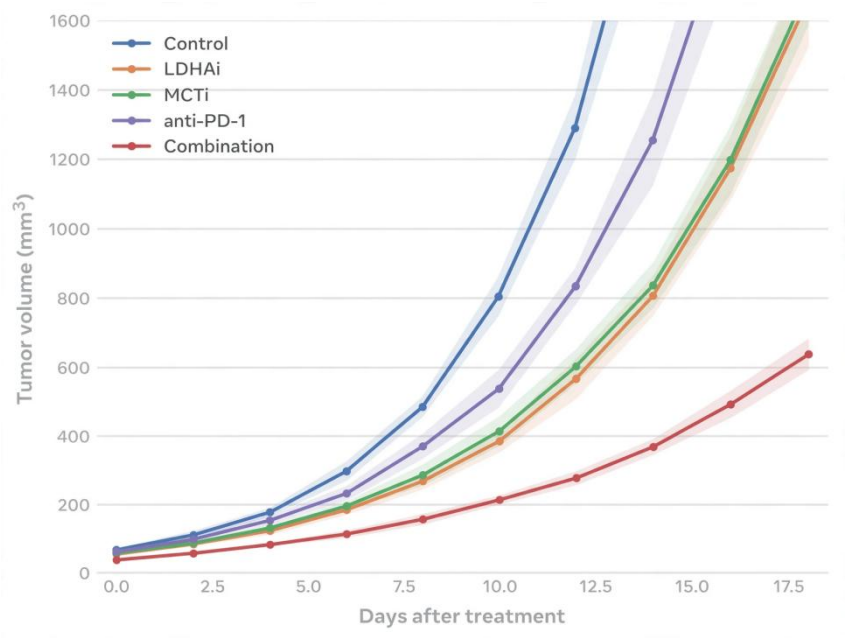
Gene	Compare with IgG	H3K18la	Enrichment factor	P-value
Pdcd1	0.08 ± 0.01	0.42 ± 0.04	5.25	<0.001
Havcr2	0.07 ± 0.01	0.31 ± 0.03	4.43	0.002
Lag3	0.09 ± 0.01	0.28 ± 0.03	3.11	0.008
Tox	0.06 ± 0.01	0.35 ± 0.03	5.83	<0.001
Ifng	0.11 ± 0.02	0.13 ± 0.02	1.18	0.412

4.5. Targeting lactate metabolism inhibits tumor growth and works together with anti-PD-1

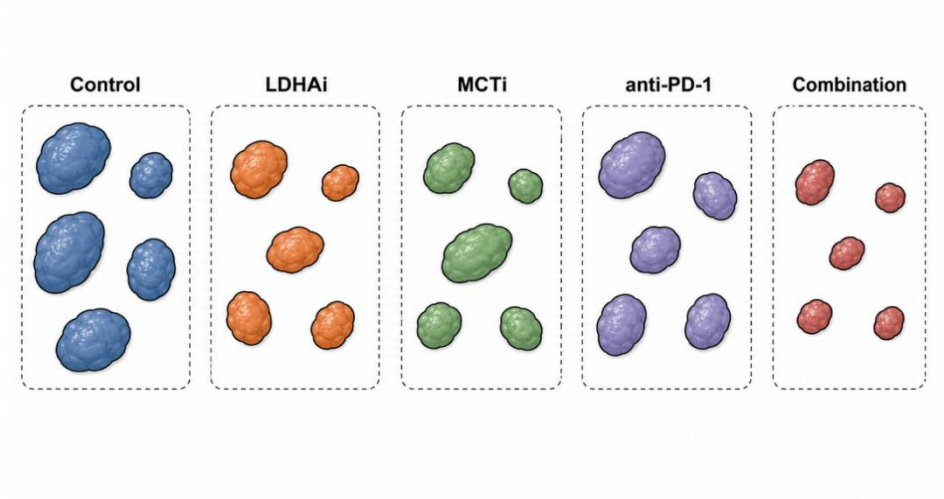
In the B16-OVA and MC38 tumor-bearing mouse models, LDHA inhibitors, MCT1/4 inhibitors, and anti-PD-1 monotherapy all inhibited tumor growth to varying degrees, while the combination treatment had the strongest tumor-suppressing effect (Table 6, Figure 5A-B). On day 18, the tumor volume in the combination treatment group was 386.5 ± 45.8 mm³, with a tumor inhibition rate of 69.0% and a median survival extended to 45 days (Table 6, Figure 5C, Table 5C). Immunohistochemistry showed that the combination treatment group had increased $CD8^+$ T cell infiltration and fewer H3K18la-positive cells in the tumor tissue (Figure 5D-E, Table 5D-E).

Figure 5

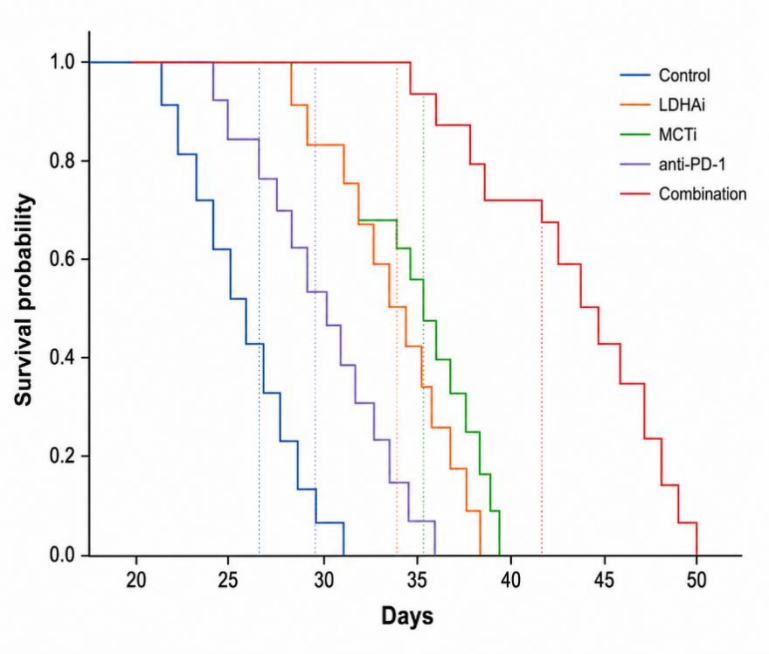
A: Tumor growth curve



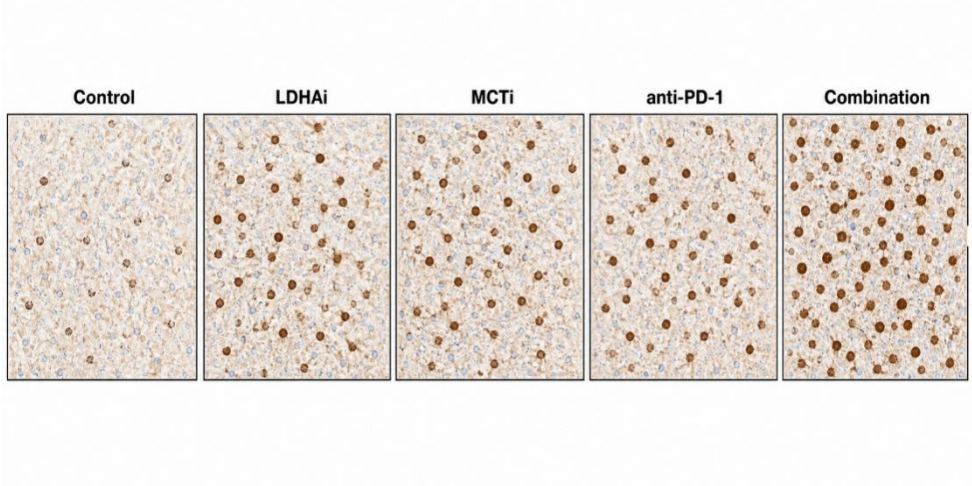
B: Endpoint tumor photos



C: Kaplan-Meier survival curve



D: Representative images of CD8⁺ T cell immunohistochemistry



E: Representative images of H3K18la immunohistochemistry

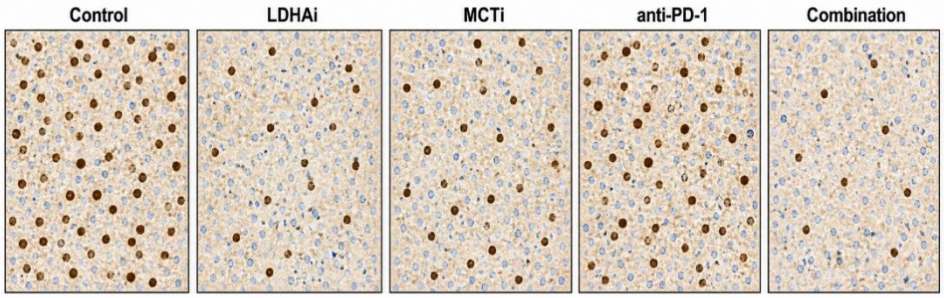


Table 5C

Kaplan-Meier survival curve

Group	Time 1	Time 2	Time 3	Time 4	Time 5	Time 6	Time 7	Time 8	Time 9	Time 10
Control	22	25	27	28	29	31	33	26	30	28
LDHAi	30	33	35	36	38	40	34	37	39	32
MCTi	31	34	35	37	39	38	36	33	40	32
anti-PD-1	28	30	31	32	34	35	29	33	36	30
Combination	38	41	43	45	47	49	42	44	46	40

Table 5D

Positive cell density

Group	Positive cell density
Control	18
LDHAi	34
MCTi	32
anti-PD-1	24
Combination	45

Table 5E

Representative images of H3K18la immunohistochemistry

Group	Positive cell density
Control	42
LDHAi	22
MCTi	24
anti-PD-1	32
Combination	13

Table 6

Analysis of tumor growth and survival in each group

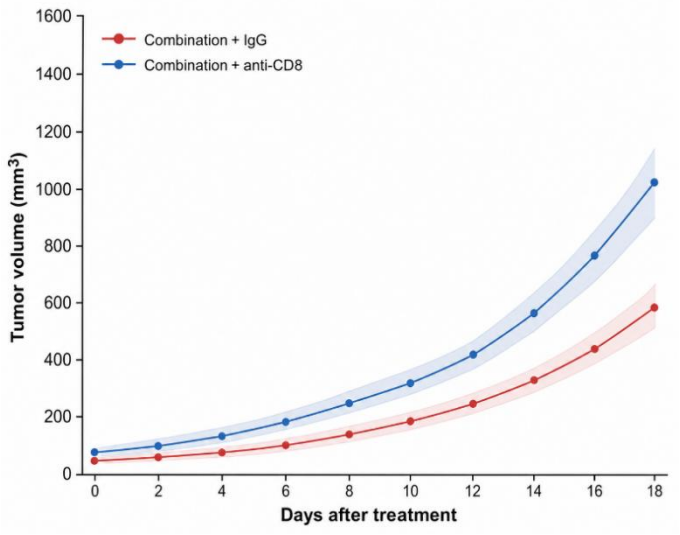
Group	Tumor volume on day 18 (mm^3)	Tumor Inhibition Rate (%)	Median survival (days)
Control	1245.6 ± 118.3	—	28
LDHAi	682.4 ± 75.6	45.2	36
MCTi	715.8 ± 81.2	42.5	35
anti-PD-1	893.7 ± 92.4	28.3	32
Combination	386.5 ± 45.8	69.0	45

4.6. $CD8^+$ T cells are key to the anti-tumor effects of lactate metabolism intervention

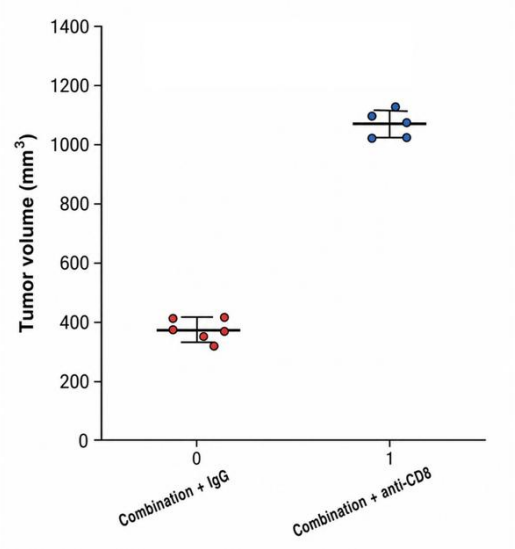
To check if $CD8^+$ T cells are necessary, we gave anti-CD8α depleting antibodies to the combination therapy group. The results showed that after removing $CD8^+$ T cells, the tumor-suppressing effect of the combo treatment dropped a lot, and the tumor size went back up close to the control group level (Table 7, Figure 6A-B, Table 6B). At the same time, the proportion of tumor-infiltrating $CD8^+$ T cells and IFN-γ^+ cells decreased significantly (Table 7, Figure 6C-D, Table 6C-D). These results suggest that the anti-tumor effect of interfering with lactate metabolism depends on $CD8^+$ T cells.

Figure 6

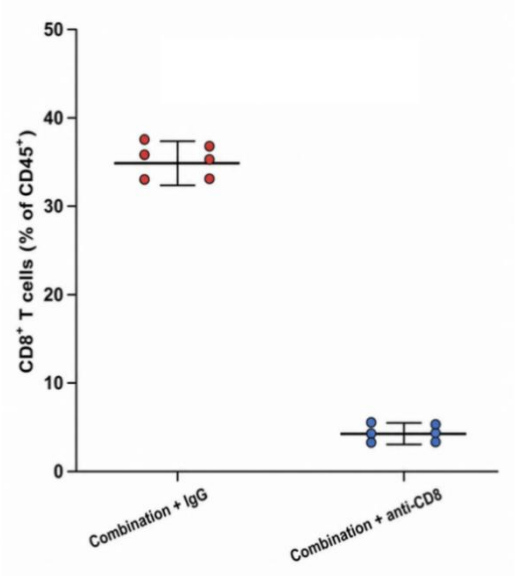
A: Tumor growth curve after $CD8^+$ T cell clearance



B: Endpoint tumor volume



C: Proportion of CD8⁺ T cells



D: Proportion of IFN-γ⁺ cells

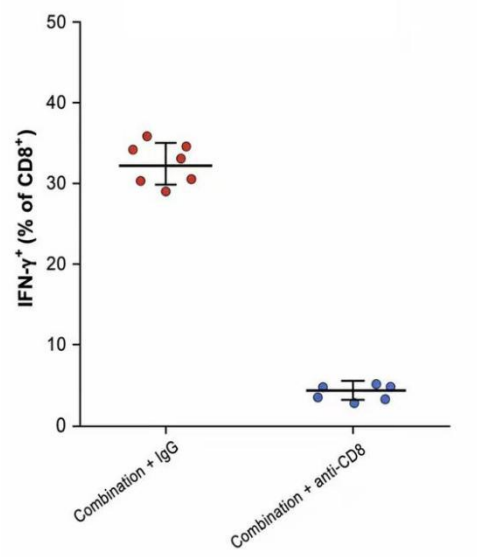


Table 6B

Final tumor volume

Group	Rep1	Rep2	Rep3	Rep4	Rep5	Rep6
Combination + IgG	368.4	392.1	345.7	412.6	378.9	401.3
Combination+anti-CD8	1042.5	1108.3	1023.7	1126.4	1068.9	1095.2

Table 6C

Proportion of $CD8^+$ T cells

Group	Rep1	Rep2	Rep3	Rep4	Rep5	Rep6
Combination + IgG	34.6	37.1	32.8	35.4	33.2	36.7
Combination + anti-CD8	4.2	3.6	5.1	4.4	3.8	4.7

Table 6D

Proportion of IFN-γ^+ cells

Group	Rep1	Rep2	Rep3	Rep4	Rep5	Rep6
Combination + IgG	31.2	34.5	29.6	32.8	30.4	33.7
Combination + anti-CD8	3.7	3.1	4.4	3.9	3.3	4.1

Table 7

The impact of $CD8^+$ T cell clearance on the effectiveness of combined therapy

Group	Tumor volume (mm^3)	$CD8^+$ T proportion (%)	IFN-γ^+（%）
Combination + IgG	386.5 ± 45.8	34.6 ± 3.0	31.2 ± 2.7
Combination+anti-CD8	1087.3 ± 102.5	4.2 ± 0.8	3.7 ± 0.6
P-value	<0.001	<0.001	<0.001

5. Discussion

This study systematically reveals the key role of lactate metabolism reprogramming in the tumor microenvironment (TME) in driving $CD8^+$ T cell exhaustion, and demonstrates that targeting LDHA or MCT1/4 can restore mitochondrial function in T cells, reverse exhaustion phenotypes, enhance anti-tumor immunity, and have synergistic effects with anti-PD-1 therapy. Mechanistically, lactate regulates transcription of depletion-related genes such as Pdcd1, Havcr2, Lag3, and Tox through histone H3K18 lactation modification, while metabolic intervention can reverse this epigenetic program. These findings link “immune metabolism” with “epigenetic immune regulation,” providing new potential targets for solid tumor immunotherapy.

5.1. Lactic acid metabolism reprogramming is an important driver of $CD8^+$ T cell exhaustion

Previous studies have shown that lactate accumulation in the TME can suppress T cell proliferation and cytokine production, and weaken the immune surveillance functions of T cells and NK cells. However, many of these studies treat lactate as an external inhibitory factor, paying relatively little attention to the metabolic reprogramming of lactate within $CD8^+$ T cells themselves. In this study, single-cell RNA sequencing and metabolomics analysis revealed that the exhausted subset of tumor-infiltrating $CD8^+$ T cells accounted for the largest proportion, with significantly increased lactate metabolism scores, along with upregulated expression of LDHA, MCT1, and MCT4, and intracellular lactate accumulation. This is in line with the idea proposed by Buck et al. (2015) that ‘the metabolic state of T cells determines their fate,’ but it goes further by directly linking lactate metabolic reprogramming to exhaustion programs. Interestingly, after inhibiting LDHA or MCT1/4, the basal and maximal ECAR of $CD8^+$ T cells decreased, while OCR and ATP production increased significantly, suggesting that interfering with lactate metabolism can push T cells from a glycolysis-dominant state to oxidative phosphorylation, thereby restoring mitochondrial function. This result echoes the findings of Bengsch et al. (2016) and Patsoukis et al. (2015) that PD-1 signaling suppresses glycolysis and harms bioenergetics, but our study goes further to show that targeting lactate metabolism can actively

reverse this metabolic defect.

5.2. Histone lactylation: A new bridge linking metabolism and exhaustion epigenetic programs

Zhang and colleagues first reported that histone lactylation is a new type of epigenetic modification linking metabolic states to gene expression, and Xiong and colleagues later found that lactylation-driven METTL3-mediated RNA m6A modification can promote myeloid cell immunosuppression. Our study extends this mechanism to exhausted $CD8^+$ T cells and finds that tumor-infiltrating $CD8^+$ T cells show increased levels of H3K18la and pan-Kla, with H3K18la significantly enriched at the promoter regions of Pdcd1, Havcr2, Lag3, and Tox. This provides direct evidence that 'metabolites maintain exhaustion programs through epigenetic modifications.' Compared to Khan's findings that TOX establishes $CD8^+$ T cell exhaustion via epigenetic programs, our work further shows that lactate, as an upstream metabolic signal, regulates the exhaustion-related transcriptional network through histone lactylation. After combined anti-PD-1 therapy, H3K18la enrichment at exhausted gene promoters decreases even more, suggesting that metabolic-epigenetic interventions could sensitize checkpoint therapy. This finding complements Chen's conclusion that NR4A transcription factors limit CAR-T cell function, indicating that maintaining the exhaustion program involves multiple layers of metabolic and transcriptional regulation.

5.3. Synergistic effects of targeting lactate metabolism with Anti-PD-1 therapy and its clinical significance

This study found that LDHA inhibitors, MCT1/4 inhibitors, or anti-PD-1 alone can partially suppress tumor growth, while combination therapy showed the strongest tumor-suppressing effect and significantly extended median survival. More importantly, after clearing $CD8^+$ T cells, the anti-tumor effect of the combination therapy almost completely disappeared, proving that $CD8^+$ T cells are the key effector cells for the efficacy of lactate metabolism intervention. This is consistent with Brand and others' conclusion that LDHA inhibition restores tumor immune surveillance, but our study further shows that targeting lactate metabolism can not only boost anti-tumor immunity on its own but also synergize with anti-PD-1 therapy. From a translational perspective, the LDHA inhibitor GNE-140 and the MCT1/4 inhibitor AZD3965 have already entered preclinical or early clinical research stages, and our study provides a theoretical basis for combining them with immune checkpoint inhibitors. Additionally, H3K18la levels might serve as a potential biomarker for predicting immune therapy response, which is worth further validation in clinical cohorts.

5.4. Innovation

The innovation of this study mainly lies in four aspects: systematically analyzing the lactate

metabolism reprogramming characteristics of tumor-infiltrating $CD8^+$ T cells themselves, shifting the research focus from tumor or myeloid cells to intrinsic T cell metabolism; for the first time showing that histone H3K18 lactylation directly regulates the transcription of genes related to $CD8^+$ T cell exhaustion, establishing a new 'lactate-lactylation-exhaustion' mechanism axis; demonstrating through genetic and pharmacological methods combined with tumor models that targeting LDHA/MCT1/4 can reverse exhaustion and boost the response to anti-PD-1 therapy; and integrating single-cell transcriptomics, metabolomics, epigenetics, and functional validation to provide multi-level, systematic evidence.

5.5. Limitations

This study has several limitations. All experiments were based on mouse tumor models. Although B16-OVA and MC38 are commonly used models in immunotherapy research, their tumor microenvironment is still different from human tumors, so the findings need further validation in humanized mice or clinical samples. LDHA and MCT1/4 inhibitors might have off-target effects. Even though we verified this using genetically knockout mice, the differences between pharmacological inhibition and gene knockout effects should be interpreted cautiously. This study mainly looked at H3K18la and pan-Kla, and it's still unclear whether other lactylation sites (like H4K12la, H3K9la, etc.) are involved in regulating exhaustion. We didn't systematically assess how interfering with lactate metabolism affects other immune cells like Tregs and myeloid cells, which could indirectly influence anti-tumor immunity. The sample size was limited, and we didn't validate in clinical cohorts, so the value of H3K18la as a biomarker still needs more research. Lastly, we didn't study how interfering with lactate metabolism affects T cell memory formation and long-term anti-tumor immunity, which should be evaluated in future studies using adoptive transfer experiments and long-term survival analyses.

6. Conclusion

This study systematically reveals the key mechanism by which lactate metabolism reprogramming drives $CD8^+$ T cell exhaustion in the tumor microenvironment. In tumor-infiltrated $CD8^+$ T cells, the expression of LDHA, MCT1, and MCT4 is upregulated, leading to intracellular lactate accumulation, accompanied by high expression of genes related to mitochondrial dysfunction and exhaustion (Pdcd1, Havcr2, Lag3, Tox). Targeting LDHA or MCT1/4 can reduce intracellular lactate levels, restore mitochondrial oxidative phosphorylation, enhance secretion of IFN-γ, TNF-α, and granzyme B, and reverse the exhaustion phenotype. Mechanistically, lactate directly regulates transcription of exhaustion-related gene promoter regions through histone H3K18 lactation modification, while metabolic intervention can reverse this epigenetic program. In the B16-OVA and

MC38 tumor-bearing models, lactate metabolism intervention significantly inhibited tumor growth and produced a synergistic effect with anti-PD-1 therapy; After clearing $CD8^+$ T cells, this efficacy almost completely disappeared, confirming that $CD8^+$ T cells are key effector cells.

The main contributions of this study are: establishing that the reprogramming of lactate metabolism in $CD8^+$ T cells themselves is a key driver of exhaustion; revealing for the first time that histone lactylation acts as a 'metabolism-epigenetics' bridge to regulate the transcription of exhaustion-related genes; and showing that targeting LDHA/MCT1/4 can reverse exhaustion and enhance the response to anti-PD-1 therapy, providing a new combination strategy for immunotherapy of solid tumors.

Future research can go deeper in the following directions: validate the correlation between lactate metabolism markers (like H3K18la) and response to immunotherapy in clinical samples and humanized mouse models, and assess their potential as predictive biomarkers; develop highly selective inhibitors, degraders, or antibody-drug conjugates targeting LDHA or MCT1/4, optimize dosing strategies, and evaluate safety; explore how lactylation-modifying enzymes (like p300/CBP, HDACs) and delactylases regulate T cell exhaustion to provide new targets for epigenetic intervention; evaluate the combined potential of lactate metabolism interventions with other immunotherapies like CAR-T, bispecific antibodies, and tumor vaccines; and analyze the effects of lactate metabolism on other immune cells like Tregs and myeloid cells to fully understand the metabolism-immune interaction network in the TME. Ultimately, the goal is to translate these basic research findings into clinically usable combination therapies and offer new ideas to improve outcomes for patients with solid tumors.

Acknowledgments

Not applicable.

Author contributions

Conceptualization, Gang Liu; methodology, Jia Wang; validation, Alena Mikalaeuna Vasiukevich; formal analysis, Biao Feng and Liqiang An; investigation, Jia Wang and Biao Feng; resources, Gang Liu and Liqiang An; data curation, Alena Mikalaeuna Vasiukevich; writing—original draft preparation, Jia Wang; writing—review and editing, Gang Liu and Alena Mikalaeuna Vasiukevich; visualization, Biao Feng; supervision, Gang Liu; project administration, Liqiang An. All authors have read and agreed to the published version of the manuscript.

Funding

Not applicable.

Data availability

Not applicable.

Declarations

Conflict of interest

The authors declare that there is no conflict of interest.

Ethics approval

Not applicable.

Consent to participate

Not applicable.

Consent for publication

All authors have given their consent.

Additional information

Received: 18 September 2026

Accepted: 19 September 2026

Published online: 8 November 2026

Publisher's Note

Wisdom Academic Press Ltd. remains neutral with regard to jurisdictional claims in published maps and institutional affiliations.

References

[1] Bengsch, B., Johnson, A. L., Kurachi, M., Odorizzi, P. M., Pauken, K. E., Attanasio, J., et al. (2016). Bioenergetic insufficiencies due to metabolic alterations regulated by the inhibitory receptor PD-1 are an early driver of CD8+ T cell exhaustion. *Immunity, 45*(2), 358-373. https://doi.org/10.1016/j.immuni.2016.07.008

[2] Brand, A., Singer, K., Koehl, G. E., Kolitzus, M., Schoenhammer, G., Thiel, A., et al. (2016). LDHA-associated lactic acid production blunts tumor immunosurveillance by T and NK cells. *Cell Metab, 24*(5), 657-671. https://doi.org/10.1016/j.cmet.2016.08.011

[3] Buck, M. D., O'Sullivan, D., & Pearce, E. L. (2015). T cell metabolism drives immunity. *J Exp Med, 212*(9), 1345-1360. https://doi.org/10.1084/jem.20151159

[4] Chen, J., López-Moyado, I. F., Seo, H., Lio, C. J., Hempleman, L. J., Sekiya, T., et al. (2019). NR4A transcription factors limit CAR T cell function in solid tumours. *Nature, 567*(7749), 530-534. https://doi.org/10.1038/s41586-019-0985-x

[5] Colegio, O. R., Chu, N. Q., Szabo, A. L., Chu, T., Rhebergen, A. M., Jairam, V., et al. (2014). Functional polarization of tumour-associated macrophages by tumour-derived lactic acid. *Nature, 513*(7519), 559-563. https://doi.org/10.1038/nature13490

[6] Fischer, K., Hoffmann, P., Voelkl, S., Meidenbauer, N., Ammer, J., Edinger, M., et al. (2007). Inhibitory effect of tumor cell-derived lactic acid on human T cells. *Blood, 109*(9), 3812-3819. https://doi.org/10.1182/blood-2006-07-035972

[7] Halestrap, A. P. (2012). The monocarboxylate transporter family—structure and functional characterization. *IUBMB Life, 64*(1), 1-9. https://doi.org/10.1002/iub.573

[8] Hanahan, D., & Weinberg, R. A. (2011). Hallmarks of cancer: the next generation. *Cell, 144*(5), 646-674. https://doi.org/10.1016/j.cell.2011.02.013

[9] Khan, O., Giles, J. R., McDonald, S., Manne, S., Ngiow, S. F., Patel, K. P., et al. (2019). TOX transcriptionally and epigenetically programs CD8+ T cell exhaustion. *Nature, 571*(7764), 211-218. https://doi.org/10.1038/s41586-019-1325-x

[10] Liu G. (2026b). Tumor microenvironment: composition, dynamic evolution, and its significance in cancer treatment. *Journal of Cancer Insights, 1*(1), 6. https://doi.org/10.66128/jci202601.1

[11] Liu, G. (2026a). The application of artificial intelligence in tumor immunotherapy: integrating multi-omics data to achieve efficacy prediction and combination strategies. *Applied Artificial Intelligence Research, 2*(2). https://doi.org/10.65455/q72yq328

[12] Liu, G., Wang, J., & An, L. (2026a). CRISPR screen and single-cell multi-omics identify a novel immune checkpoint on tumor-infiltrating regulatory T cells. *Injury and Rehabilitation Care, 2*(1). https://doi.org/10.63808/irc.v2i1.525

[13] Liu, G., Wang, J., & An, L. (2026b). Gut microbiota-derived butyrate induces trained immunity in intestinal macrophages to potentiate antitumor immunity. *Biology and Medical Engineering, 2*(1). https://doi.org/10.63808/bm.v2i1.523

[14] Liu, G., Wang, J., & An, L. (2026c). Mitochondrial DNA sensing reshapes the tumor immune microenvironment via cooperative cGAS-STING activation and ferroptosis. *Global Health Care, 2*(1). https://doi.org/10.63808/ghc.v2i1.524

[15] Liu, G., Wang, J., & Zhu, J. (2026d). Explainable spatial AI analyzes tumor-immune interactions to predict immunotherapy outcomes and identify new targets. *Intelligent & Human Futures, 2*(3). https://doi.org/10.63808/ihf.v2i3.510

[16] Liu, G., Wang, J., & Zhu, J. (2026e). Using multimodal foundational models to predict neoantigen immunogenicity and vaccine effectiveness across different tumor types. Global Health Care, 2(3). https://doi.org/10.63808/ghc.v2i3.498

[17] Patsoukis, N., Bardhan, K., Chatterjee, P., Sari, D., Liu, B., Bell, L. N., et al. (2015). PD-1 alters T-cell metabolic reprogramming by inhibiting glycolysis and promoting lipolysis and fatty acid oxidation. *Nat Commun, 6*, 6692. https://doi.org/10.1038/ncomms7692

[18] Vardhana, S. A., Hwee, M. A., Berisa, M., Wells, D. K., Yost, K. E., King, B., et al. (2020). Impaired mitochondrial oxidative phosphorylation limits the self-renewal of T cells exposed to persistent antigen. *Nat Immunol, 21*(9), 1022-1033. https://doi.org/10.1038/s41590-020-0725-2

[19] Warburg, O. (1956). On the origin of cancer cells. *Science, 123*(3191), 309-314. https://doi.org/10.1126/science.123.3191.309

[20] Wherry, E. J. (2011). T cell exhaustion. *Nat Immunol, 12*(6), 492-499. https://doi.org/10.1038/ni.2035

[21] Xiong, J., He, J., Zhu, J., Pan, J., Liao, W., Ye, H., et al. (2022). Lactylation-driven METTL3-mediated RNA m6A modification promotes immunosuppression of tumor-infiltrating myeloid cells. *Mol Cell, 82*(9), 1660-1677.e10. https://doi.org/10.1016/j.molcel.2022.02.033

[22] Zhang, D., Tang, Z., Huang, H., Zhou, G., Cui, C., Weng, Y., et al. (2019). Metabolic regulation of gene expression by histone lactylation. *Nature, 574*(7779), 575-580. https://doi.org/10.1038/s41586-019-1678-1